SCIENTIFIC REPORTS

OPEN

SUBJECT AREAS:
MATERIALS SCIENCE
MATERIALS FOR DEVICES

Received
15 October 2013

Accepted
9 January 2014

Published
3 February 2014

Correspondence and requests for materials should be addressed to L.H.Z. (lhzhu63@hust.edu.cn) or H.Q.T. (hqtang62@aliyun.com; THQ@mail.scuec.edu.cn)

Novel One-pot Fabrication of Lab-on-a-Bubble@Ag Substrate without Coupling-agent for Surface Enhanced Raman Scattering

Jizhou Jiang[1,2], Lei Ou-Yang[1], Lihua Zhu[1], Jing Zou[3] & Heqing Tang[2]

[1]College of Chemistry and Chemical Engineering, Huazhong University of Science and Technology, Wuhan 430074, P.R. China, [2]Key Laboratory of Catalysis and Materials Science of the State Ethnic Affairs Commission and Ministry of Education, College of Chemistry and Materials Science, South Central University for Nationalities, Wuhan 430074, P.R. China, [3]School of Chemical Engineering and Pharmacy, Wuhan Institute of Technology, Key Laboratory for Green Chemical Process of Ministry of Education, Wuhan 430073, P.R. China.

Through in-situ reduction of silver nitrate without using any coupling-agent, a substrate for surface-enhanced Raman scattering (SERS) was prepared by coating silver on hollow buoyant silica microspheres as a lab on a bubble (LoB). The silver coated LoBs (LoBs@Ag) floated on surface of a solution could provide a very convenient platform for the detection of target molecules in the solution. The LoBs@Ag substrate not only immobilized well-distributed Ag nanoparticles on the surface LoBs, but excluded the interference of coupling agents. This yielded high-resolution SERS spectra with excellent reproducibility. The adsorption of crystal violet (CV) on the LoBs@Ag substrate was investigated by means of SERS combined with density functional theory (DFT) calculations. The LoBs@Ag substrate exhibited a remarkable Raman enhancement effect for CV with an enhancement factor of 6.9×10^8 and wide adaptability from dye, pesticide to bio-molecules. On the basis of this substrate, a simple and sensitive SERS method was proposed for the determination of trace organic pollutants or bio-molecules.

Surface-enhanced Raman scattering (SERS) consists on the enhancement of the Raman scattering intensity by molecules in the presence of a nanostructured metallic surface. Because of high sensitivity and unique performances providing all the vibrational information of the target molecule[1–3], SERS has become a very active field in the areas of materials and analytical sciences[4,5]. The early reported SERS substrates were Au, Ag and Cu electrodes[6,7]. The ability to support the excitation of surface-plasmons in the visible region is a characteristic shared by Au, Ag and Cu, and a great part of the enhancement in SERS was early attributed to the resonances[8,9]. The excitation of surface-plasmons causes an enhancement in the electric-field localized around the nano-sized metallic structures, leading to both the excitation light and the scattered radiation to be surface-enhanced. Now, metallic nanoparticles (NPs), such as Au, Ag and Cu NPs, were reported as substrates. However, it is generally necessary for the NP-based SERS system to make optimizations of many parameters, since both the frequency and magnitude of the maximum field enhancement are strongly dependent on the shape, size and arrangement of the metallic nanofeatures[10–13]. As for the substrate, its sensitivity is primarily important for SERS measurements. Recent developments have greatly improved the sensitivity of SERS substrates based on NPs alone, functionalized metal NPs and possible anisotropic structures. Yang et al.[14] prepared SERS-active gold lace nanoshells with biocompatible amphiphilic polyurethanes as template, and observed that the nanoshells acted as single particle "hotspots" in suspension to monitor the loading and releasing of pyrene as a model of hydrophobic drugs. Han et al.[15] reported the use of silver-coated gold (Au@Ag) NPs as stand-alone-particle Raman amplifiers for the identification and detection of pesticide residues on various fruit peels, and found that the Raman enhancement of Au@Ag NPs was about two orders of magnitude stronger than those of bare Au and Ag NPs. Peng et al.[16] fabricated copper oxide functionalized silver nanowires for SERS, which presented high sensitivity to biomolecules (such as: D-glucose and adenine molecules) due to the enhanced surface roughness of silver nanowire and the molecule capture capability of copper oxide NPs. According to the difference in adsorption of DNA onto Ag NPs surfaces, Graham et al.[17] used Ag NPs as SERS substrates to directly detect specific polymerase chain reaction

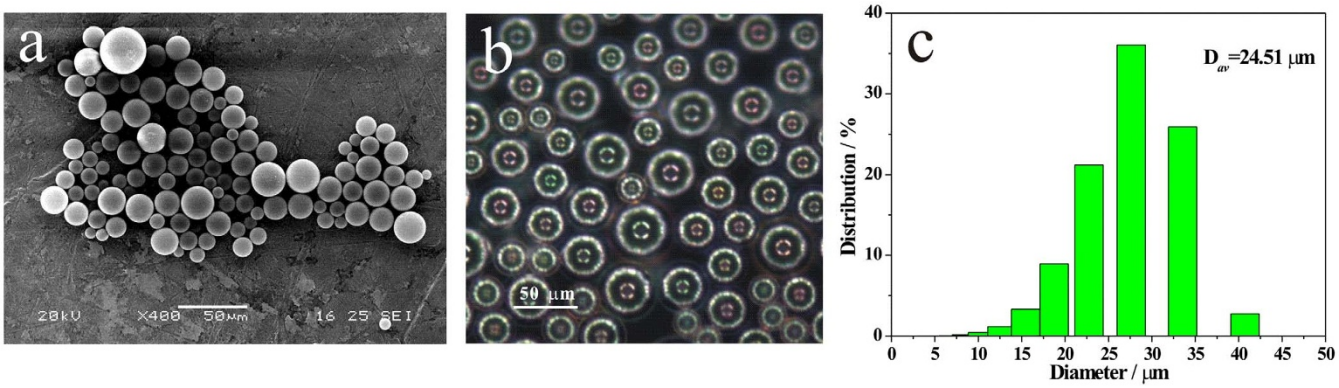

Figure 1 | **SEM image (a), normalized optical image (b) and size distribution (c) of LoBs.**

products. Although these methods provided the substrates with a high SERS sensitivity, the SERS responses of the obtained substrates have a relatively low reproducibility due to the Brownian motion of nanoparticles in solution. Individual metallic NPs often move into and out of the focused laser beam, leading to the instability SERS signal of analyte absorbed on the surface of metallic NPs.

To overcome the poorer reproducibility of mobile NPs, a concept of a lab-on-a-bubble (LoB) was proposed as a class of SERS substrate materials[18]. The LoB material is prepared by coating Au or Ag NPs on hollow buoyant SiO_2 microspheres by using a silane coupling agent such as aminopropyltriethoxysilane (APTES). The LoB concept is centered on low-density microspheres that utilize buoyant force to drive assay separation, while the metallic NPs on the buoyant particles act as SERS nanosensors[19]. LoBs@APTES@Ag substrates are indifferent of Brownian movement, and serve as a convenient platform to directly detect the target molecules in solution, without draining water. Aminopropyltrimethoxisilane (APTMS), mercaptopropyltrimethoxysilane (MPTMS), dopamine (DA) and polydopamine (PDA) were also used as coupling agents for surface modification[20,21]. The use of a coupling agent strengthens the interfacial adhesion of NPs on SiO_2 microspheres, but the silylation process is time-consuming. More seriously, the functional groups of the coupling agents may interfere on the Raman signals of the target molecules. Wang et al. reported that Ag NPs assembled on mica showed SERS effects with p-mercaptoaniline as a probe, and the assembling of Ag NPs (with an average size of 41 nm) on mica was achieved by electrostatic interaction between negatively-charged Ag NPs (due to the surface $-COO^-$) and the positively-charged mica surface[22]. In the preparation, the mica sheets were required to be freshly peeled, which is unfavorable to massive preparation of the composite as a SERS substrate material.

To keep the advantages of LoBs materials in handling aqueous samples and avoid the weakness of coupling agents, we proposed a simple method in this work, in which well-distributed Ag NPs were directly grown on the surface of commercial 3 M glass floatation bubbles as substrates without using any coupling agent for SERS measurements. CV was used as a probe molecule to evaluate the SERS performance of the LoBs@Ag substrate. In comparing with normal Raman scattering, the LoBs@Ag substrate provided an enhancing factor as high as 6.9×10^8 for CV molecules. A linear correlation was established between the measured SERS intensity and the concentration of CV in the range of $2.5 \times 10^{-8} \sim 2.5 \times 10^{-6}$ mol L^{-1}. The excellent reproducibility and stability of LoBs@Ag substrate were confirmed by comparing the SERS activities of different substrates. Adaptability of the LoBs@Ag substrate for a wide range of systems starting from dye (CV), pesticide (paraquat) to bio-molecules (DA and guanine) is demonstrated.

Results

A typical SEM image of commercial LoBs is shown in Fig. 1a. The LoBs are fairly smooth and spherical in shape with diameters of 10 ~ 40 μm. Fig. 1b presents a normalized optical image of LoBs recorded in the scanning confocal microscope, which reveals that LoBs are composed of hollow microspheres with an average diameter of 25 μm. Fig. 1c shows the size distribution of LoBs and indicates that the size of the samples is mainly between 15 and 40 μm. The mean diameter was 24.51 μm. This result is concordant with the SEM image.

Fig. 2 shows the processes of preparing the LoBs@Ag substrate materials. Firstly, the LoBs were washed and flotated in Milli-Q water. At this time, the zeta potential value of flotated LoBs was −30.3 mV (pH = 8.9), indicating that the LoBs had a negatively charged surface. After adding Ag^+ ions, the zeta potential was up to −24.3 mV at the same pH, implying that Ag^+ ions were adsorbed on the surface of LoBs through electrostatic attraction. At the last step, the adsorbed Ag^+ ions were then reduced by adding $NaBH_4$, giving the product of LoBs@Ag after properly washing.

The morphologies and chemical compositions of LoBs and LoBs@Ag are compared in Fig. 3. Before the deposition of Ag, the LoBs clearly display its very smooth microsphere surface (Fig. 3a) in accordance with the SEM observation (Fig. 1a). After the deposition of Ag, the LoBs@Ag particle shows a coarse surface (Fig. 3b). Fig. 3c shows the high-resolution SEM image of LoBs@Ag, which presents well-distributed Ag NPs with a uniform diameter of ~12 nm. As shown in Fig. 3d, indeed, the EDS spectrum of LoBs@Ag demonstrates obvious signals of Ag element. A comparison between the

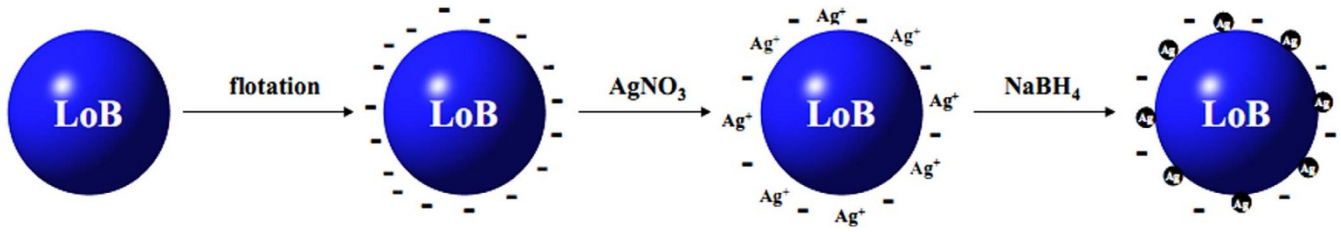

Figure 2 | **A schematic diagram for the preparation of LoBs@Ag.**

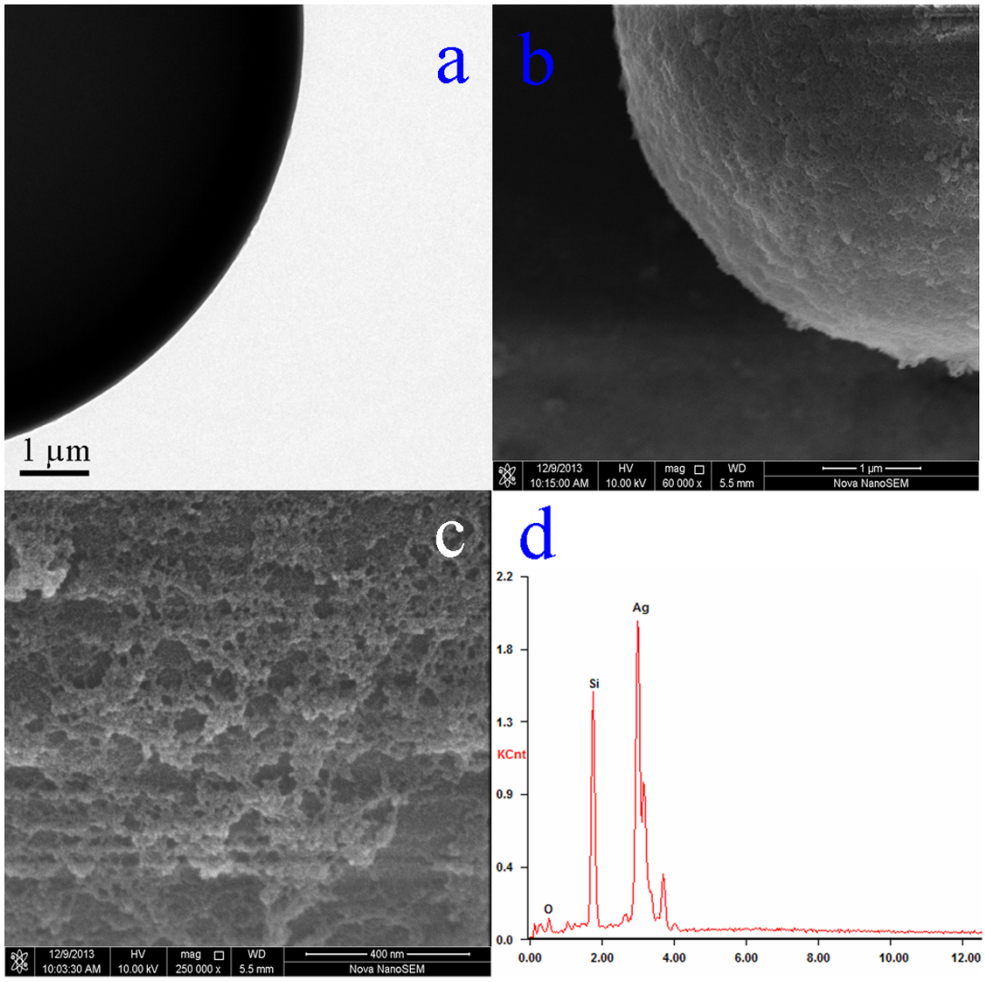

Figure 3 | **TEM image of LoBs (a), high-resolution SEM images of LoBs@Ag (b, c), and EDS spectrum (d) of LoBs@Ag.**

XRD patterns of the LoBs@Ag and LoBs (See Fig. S1) further indicates the coating of metallic Ag on the surface of LoBs due to the appearance of strong peaks from Ag. From the XRD peak intensity, the mean crystallite size of Ag particles was estimated about 15 nm, well consistent with the SEM image (Fig. 3c). Normalized UV-Vis absorption spectrum of the Ag colloid obtained with $NaBH_4$ as the reducing agent was also recorded, and then its particle size analysis was conducted (Figs. S2 and S3). The average diameter of the Ag colloid was about 11 nm, in accordance with the result of high-resolution SEM observation. The above-mentioned results indicated that the Ag NPs on the surface of LoBs displayed a monodisperse distribution without marked agglomeration. Therefore, the LoBs@Ag substrate with uniformly-distributed Ag NPs is successfully prepared without using any coupling agent. This preparation method is straightforward, time-saving and cost efficient.

Fig. 4a shows the optical image of CV powder under ×500 bright field. The color of CV powder presents gray-blue and yellow under the Raman microscopic conditions. The optimized geometry of CV

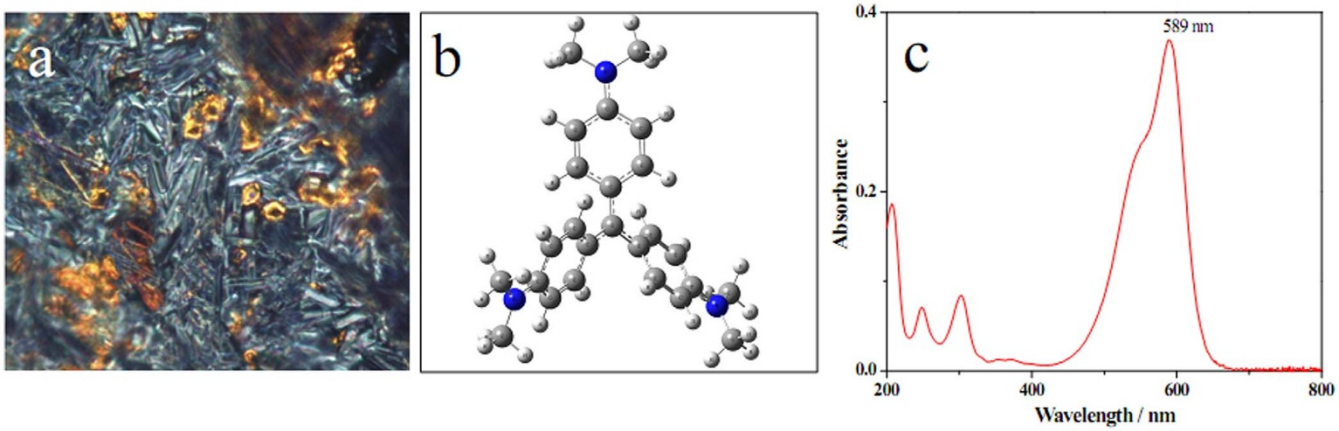

Figure 4 | **Optical image (×500 bright field) of CV powder (a), optimized CV geometry using B3LYP/6-311 + G(d) (b), and UV-vis spectrum of CV solution (5×10^{-6} mol L^{-1}) (c).**

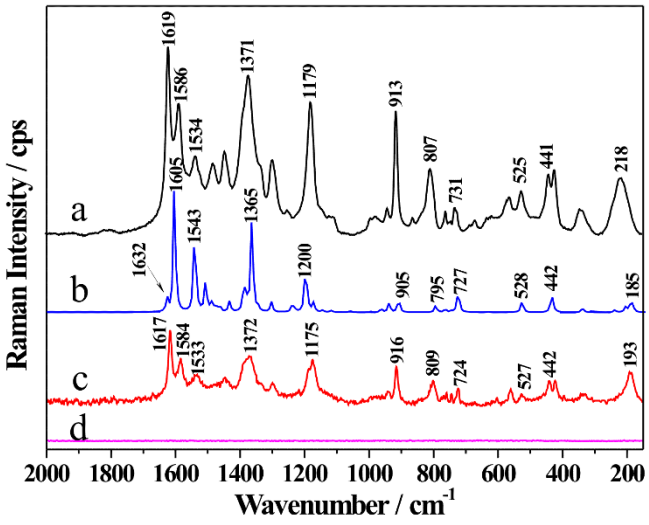

Figure 5 | SERS spectrum of CV (2.5×10^{-6} mol L^{-1}) adsorbed on LoBs@Ag (a), theoretical CV Raman spectrum obtained with DFT calculations by using 6-311 + G(d) basis sets and scaled by 0.96 (b), normal Raman spectra of CV powder (c) and CV solution (2.5×10^{-6} mol L^{-1}) (d).

molecule was performed at the density functional theory (DFT) B3LYP/6-311 + G(d) level. The DFT result shows that the optimized structure of CV exhibits a propeller-like shape with D_3 symmetry (Fig. 4b) and that three dimethylanilinium groups are linked to a central carbon atom. It is well known that a symmetric fundamental vibration usually gives a strong Raman line due to it generally accompanied with a great change in polarizability[23]. Thus, a CV molecule should present a strong Raman signal. Moreover, the excitation laser line 532 nm is within the strong absorption band of CV with λ = 589 nm (Fig. 4c). This allows much easier occurrence of resonance enhancement Raman of CV. Therefore, we choose CV as the probe molecule to investigate the SERS activities of substrates in our experiments.

Fig. 5 shows the SERS, the DFT calculated and normal Raman (powder and solution) spectra of CV. No obvious peak was observed in the normal Raman spectrum of CV solution (Fig. 5d), but the normal Raman spectrum of CV powder (Fig. 5c) shows plentiful peaks. All of these peaks are significantly enhanced in intensity in the case of the SERS spectrum (Fig. 5a), demonstrating that there is a remarkable Raman enhancement effect on the LoBs@Ag surface. By comparing the DFT calculated spectrum (Fig. 5b) with the SERS spectrum (Fig. 5a) and the normal Raman spectrum of CV powder (Fig. 5c), it was found that the calculated Raman spectrum matched the experimental results very well, which are in good agreement with that reported in previous works[24–26].

Fig. 6 presents SERS spectra of different substrates of LoBs@Ag, LoBs@PDA@Ag-R, LoBs@PDA@Ag-A, LoBs@APTES@Ag and Ag colloid. It was easily found that there were strong Raman vibrational peaks with well defined and high resolution on LoBs@Ag as the substrate. The LoBs@Ag substrate exhibited strong Raman enhancing effect in comparison with other substrates.

Quantification of the enhancement factor (EF) of a SERS substrate needs some assumptions since the number of adsorbed molecules is poorly defined[27,28]. In this work, we assume that CV molecules are uniformly adsorbed on the LoBs@Ag surface. EF was calculated by using the standard formula[29],

$$EF = I_{SERS} * C_{NR} / I_{NR} * C_{SERS}$$

where I_{SERS} and I_{NR} are the integral intensity obtained by SERS and normal Raman scattering measurements, respectively. C_{SERS} and C_{NR} are the concentration of molecules used for SERS and normal Raman scattering measurements, respectively. The most intense peak was considered for EF calculation, and the EF values of different substrates were obtained (Table S1). Because some broad peaks appeared around 1619 cm^{-1} would make it difficult to distinguish the individual integrated intensity in the SERS spectra on the LoBs@PDA@Ag-A and LoBs@APTES@Ag substrates for CV, the curves fitting of the SERS spectra was conducted (Fig. S4) on the basis of soft interference cancellation. Obviously, the LoBs@Ag substrate provided an enhancing factor as high as 6.9×10^8 for CV, which is much more than that provide by Ag colloid ($\sim 3.1 \times 10^6$) and the Ag-coated

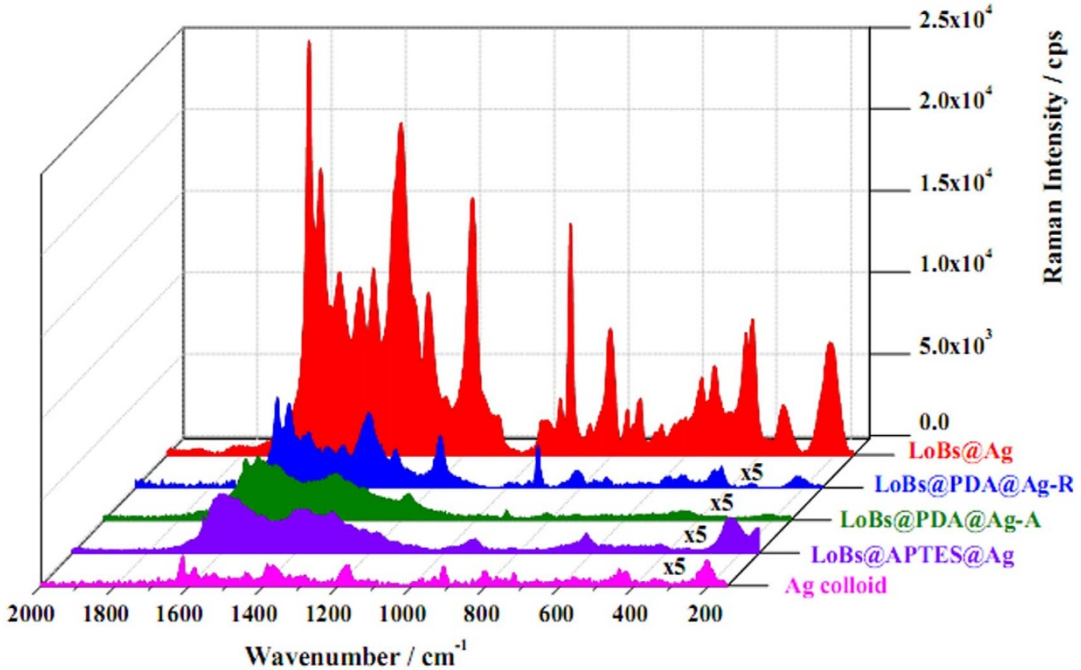

Figure 6 | Comparison of SERS activity of different substrates of LoBs@Ag, LoBs@PDA@Ag-R, LoBs@PDA@Ag-A, LoBs@APTES@Ag and Ag colloid. The concentration of CV probe was 2.5×10^{-6} mol L^{-1}.

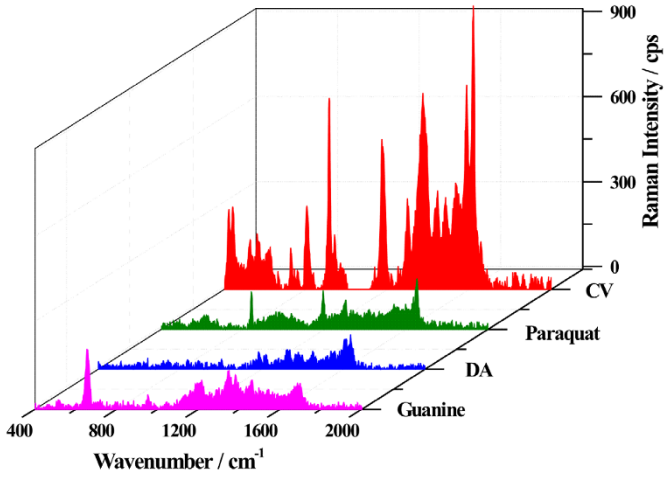

Figure 7 | SERS spectra of CV (2.5×10^{-7} mol L^{-1}), paraquat (1.0×10^{-4} mol L^{-1}), DA (1.0×10^{-4} mol L^{-1}) and guanine (2.0×10^{-5} mol L^{-1}) on the LoBs@Ag substrate.

LoBs with the use of coupling agents (about 2×10^7). Therefore, the LoBs@Ag as a substrate yields the most strongly enhanced SERS responses.

To check the wide adaptability of LoBs@Ag as a SERS substrate, other analytes were investigated, including paraquat as a pesticide, guanine and DA as two small bio-molecules (see their chemical structures in Fig. S5). As shown in Fig. 7, these substances showed SERS signals. The enhancement factors (Table S1) were evaluated to be 7.5×10^5, 6.4×10^6 and 5.7×10^5 for paraquat, guanine and DA, respectively. These results indicated that the LoBs@Ag substrate possessed wide adaptability as a SERS substrate.

To evaluate the reproducibility of LoBs@Ag substrate, SERS spectra of CV were measured by using different batches LoBs@Ag as the substrate. Fig. 8a illustrates the SERS spectra of CV (2.5×10^{-6} mol L^{-1}) on eight different batches of LoBs@Ag synthesized under the same conditions. The obtained spectra from different batches substrates overlapped extremely well. The relative standard deviations (RSD %) of the Raman intensity at 1619 cm^{-1} was less than 9.6%. This indicates that the LoB@Ag substrate exhibites good reproducibility. Furthermore, since the illumination laser spot size of DXR Raman spectrometer (Φ = 1.1 μm) is much smaller than the diameter of LoB (Φ = 25 μm), only small parts of Ag particles on the surface of flotated LoB@Ag lies in the illuminated area. Therefore, compared to traditional Ag colloid solutions (10 to 60 nm) with Brownian movement, the variation is quite small. At the same time, the stability of LoBs@Ag substrate was evaluated by comparing the SERS spectra of CV on the LoBs@Ag with different depositing time (0–96 h). As shown in Fig. 8b, no marked differences were observed between the recorded spectra, and the RSD value of the Raman intensity at 1619 cm^{-1} was about 6.2%. Therefore, the LoBs@Ag substrate exhibited excellent reproducibility and stability.

Fig. 9a presents the SERS spectra of CV at different concentrations on LoBs@Ag, and Fig. 9b shows a good linear relationship between the measured SERS intensity (at 1619 cm^{-1}) and the concentration of CV. Each data is the average value after at least 50 measurements and the relative standard deviation (RSD, %) of each group of the data was about 10%. Fig. 9b indicates that there is a wide linear response range from 2.5×10^{-8} to 2.5×10^{-6} mol L^{-1} with a limit of detection (LOD) of about 7.5×10^{-9} mol L^{-1}. This result is superior to the reported value that a linear response range is from 1.3×10^{-6} to 2.6×10^{-5} mol L^{-1} on Q-SERS substrates (Nanova Inc., Columbia, MO, USA) within CV solution[24] and that a value of LOD is about 5.0×10^{-7} mol L^{-1} for CV on electrochemically roughened silver substrates[30]. Therefore, the semiquantitative analysis of organic pollutants with LoBs@Ag as SERS substrates is feasible.

Discussion

To investigate the interaction between the probe molecules CV and LoBs@Ag substrate surface, the Raman spectra were collected by means of SERS combined with density functional theory (DFT) calculations. The assignments of Raman bands of CV obtained from the experiment and calculations are listed in Table 1 (Fig. S6 showed the calculated six main vibration modes of CV). The peak at 913 cm^{-1} in the SERS spectrum corresponds to the 916 cm^{-1} peak in the Raman spectrum. This relatively strong peak is assigned to the phenyl ring breathing mode. No obvious broadening of peak shape or apparent shift in peak position was observed for the phenyl ring breathing mode before and after the adsorption of CV, indicating that the adsorption orientation through aromatic ring can be excluded[31].

The peaks at 1617 and 1584 cm^{-1} in the normal Raman spectrum of CV powder, assigned to the C-phenyl in-plane antisymmetric stretching mode, are intensely enhanced and shifts to 1619 and 1586 cm^{-1} in the SERS spectrum, respectively. The observed frequency shift is due to its substitute sensitivity[32]. The peak at 1179 cm^{-1} in the SERS spectrum, corresponding to the peak at 1175 cm^{-1} in the normal Raman

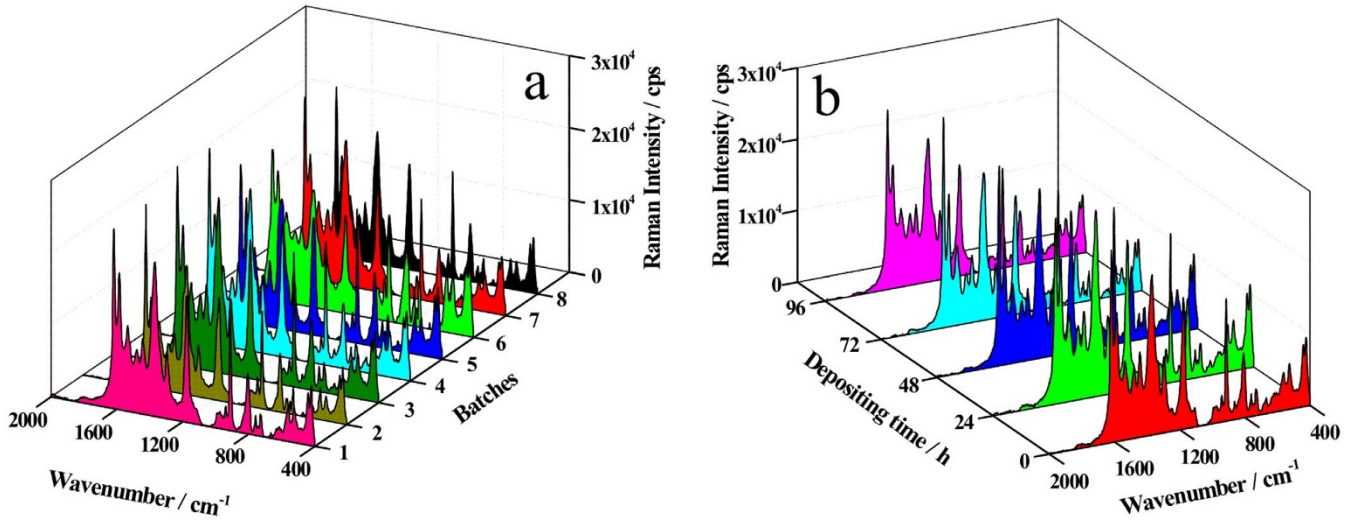

Figure 8 | SERS spectra of CV (2.5×10^{-6} mol L^{-1}) on eight different batches LoBs@Ag synthesized under the same conditions (a) and on the LoBs@Ag with different depositing time of 0, 24, 48, 72 and 96 h (b).

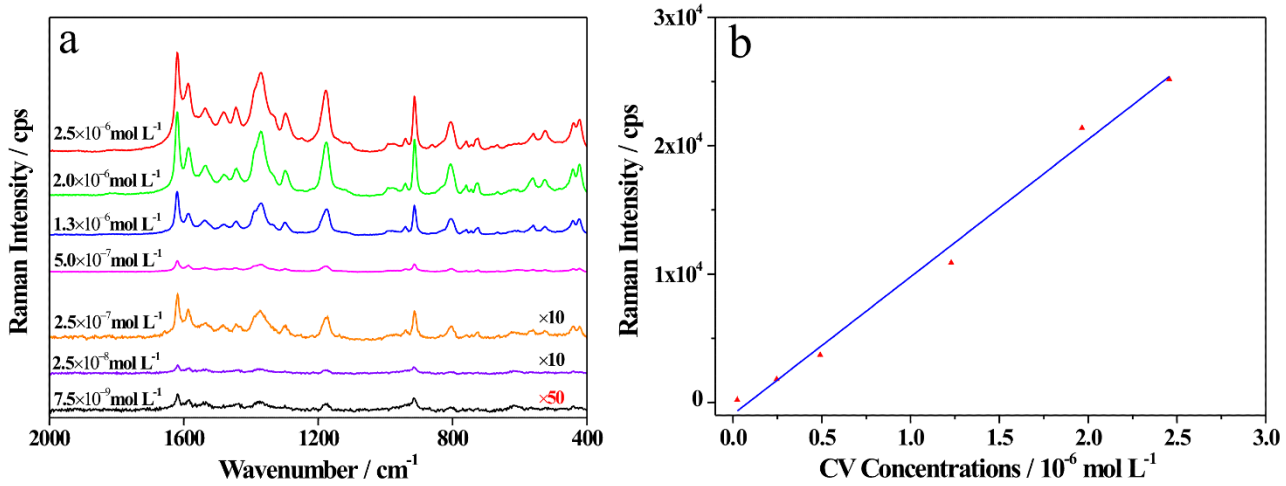

Figure 9 | (a) SERS spectra of CV at different concentrations on LoBs@Ag and (b) the relationship between CV concentration and Raman intensity at 1619 cm^{-1}.

spectrum of CV powder and assigned to the C-phenyl, C-H in-plane antisymmetric stretching mode, is intensively enhanced.

On the other hand, the peak at 809 cm^{-1} in the normal Raman spectrum of CV powder, assigned to the phenyl-H out-of-plane antisymmetric bending mode, is intensely enhanced and shifted to 807 cm^{-1} in the SERS spectrum. The phenyl-C-phenyl out-of-plane antisymmetric bending mode at 442 cm^{-1} in the normal Raman spectrum of CV powder is enhanced and shifted to 441 cm^{-1} in the SERS spectrum. On the basis of the surface selection rule[33,34], the enhancements of both in-plane and out-of-plane modes suggest that phenyl rings of CV are tilted with respect to the LoBs@Ag surface (Fig. S7).

Moreover, in the SERS spectrum, there is a new strong peak at 218 cm^{-1} (Table 1), which is attributed to the N-Ag symmetric stretching mode. The appearing of this peak indicates that there is an interaction between CV and LoBs@Ag surface through the N-Ag bonding, which is further confirmed by DFT calculations (Section S2 and Fig. S8, Supporting Information). As a result, several peaks concerned with the N atoms, such as 527, 731, 1373 and 1534 cm^{-1}, are slightly blue-shifted in comparison with their corresponding peaks in the normal Raman spectrum of CV powder. The blue shift of these vibrations may be due to the electron donor effect of CV molecule[32], in accordance with the DFT calculations that the electronic structure of CV is changed as a result of charge transfer from CV to the Ag_4 cluster surface, causing a blue shift of some vibrational modes.

Table 1 | Assignments of Raman bands of CV in the experiment and calculations

Raman	SERS	DFT cal.[a]	Assignment[b]
1617	1619	1632	ν_{as}, ip, C-φ
1584	1586	1605	ν_{as}, ip, C-φ
1533	1534	1543	ν_{as} φ-N
1370	1373	1365	ν_{as}, φ-C-φ, C-N
1175	1179	1200	ν_{as}, ip, C-H, C-φ
916	913	905	ω
809	807	795	$\gamma_{as,oop}$, φ-H
724	731	727	ν_s C-N-C
524	527	528	γ_{as} C-N-C
442	441	432	$\gamma_{as,oop}$, φ-C-φ
193	---	185	ν_{as}, oop, C-H
---	218	---	ν_s Ag-N

[a]The frequencies are predicted at the B3LYP/6-311 + G(d) level and scaled with 0.96.
[b]All values in cm^{-1}; ν, stretch; s, symmetric; as, antisymmetric; ip, in-plane; γ, bend; oop, out-of-plane; φ, phenyl; ω, ring breathing.

Generally speaking, both electromagnetic enhancement and chemical enhancement contribute to the total SERS enhancement. A large enhancement (about 10^5) is from the electromagnetic enhancement mechanism, because Ag NPs on the surface of LoBs@Ag substrate can convert incident light into nanoscale confined and strongly enhanced optical fields ('hot spots')[35]. The charge-transfer (chemical) enhancement leads to frequency shifts of the adsorbed group that are linked directly with the metal surface[36]. As discussed above, the vibrational wavenumbers associated with N atoms have a blue shift. This indicates that charge-transfer enhancement has a contribution to the total enhancement, in accordance with that the absorption enhancement of CV at 532 nm relates to chemical resonance. Hence it was concluded that CV molecules adsorbed on LoBs@Ag through its N atoms coordinating to the surface silver with phenyl rings of CV being tilted to the LoBs@Ag surface and that both electromagnetic enhancement and charge transfer contribute to the total SERS enhancement.

To further confirm the enhancing effect of the LoBs@Ag substrate, we have compared its SERS activity with that of other substrates under the same measurement conditions. As shown in Fig. 6, almost all vibrational modes of CV appeared on Ag colloid as the substrate, but the intensity of the characteristic peaks of CV on Ag colloid is the lowest in comparison with other substrates. This is mainly because the unimmobilized Ag colloid particles are movable and the numbers of Ag NPs in a focused laser beam are small due to the Brownian motion of Ag NPs.

It is easily found that all the substrates being prepared by fixing Ag NPs on the surface of LoBs with the use of coupling agents (LoBs@APTES@Ag, LoBs@PDA@Ag-A and LoBs@PDA@ Ag-R) provide a Raman enhancing effect. This is in good agreement with that reported on the literatures[37,38]. The increased Raman enhancing effect is attributed to the immobilization of Ag NPs on the surface LoBs by the coupling-agent-mediated Ag adsorption. More interesting, in comparison with the above three substrates, the LoBs@Ag substrate being obtained without any coupling agent provided a much more strong enhancing effect.

It is important to explain the above-mentioned observations. Firstly, the surface functional groups of the substrates obtained with and without using the coupling agent may influence the SERS effect of the substrates. Accordingly, we recorded FT-IR transmission spectra of the related substrates (Fig. S9). According to the IR spectroscopy of silica[39–42], the band at 798 cm^{-1} is due to Si-O-Si symmetric stretching vibrations, which are attributed to the ring structure of the SiO_4 tetrahedra. The band near 1039 cm^{-1} is associated with the Si-O-Si asymmetric stretching vibration. A peak at 1389 cm^{-1} was

observed in the spectrum of LoBs, and this peak exhibited a slight blue-shift after modification by Ag, PDA or APTES. This absorption feature is due to the O-H bending deformation in -COOH[43], or the consequence of the weak bonding of residual APTES and PDA molecules[44]. It has reported that stand-alone APTES generally shows a doublet at 1100 and 1075 cm^{-1} for the Si-O-C stretching mode[45]. In our present work, the characteristic bands of APTES disappear after the formation of LoBs@APTES@Ag but the occurrence of the characteristic band of the Si-O-Si backbone clearly confirmed the condensation of APTES into the polymeric phase. The characteristic peak being attributed to the Si-O-Si stretching vibration also shifted from 1039 to 1042 cm^{-1}. All these observations indicated that the surface of the floated LoBs had been functionalized by Ag, PDA or APTES. From the schematic representations of the routes of synthesizing the related substrate materials (Fig. S10(a–c)), it is easily understood that some chemical bonds (-Si-O-Si-, or O-H) are formed between coupling agents and LoBs, which is well consistent with the observation from the FT-IR spectra. However, the observed difference of functional groups could not provide direct evidence to prove the different SERS effects of the related substrates.

Depending on the preparation conditions, secondly, the size distribution, aggregation status and coverage density of Ag NPs on LoBs may influence the Raman responses of the different substrates. It is possible to evaluate the particle size and aggregation status of Ag NPs by analyzing the UV-vis absorption spectra of the NP suspensions. In the UV-vis absorption spectrum of the Ag colloid prepared with $NH_2OH{\cdot}HCl$ as the reducing agent (Fig. S11), a strong absorption peak was observed at about 422 nm, being to the surface plasmon resonance[46,47]. However, the UV-vis absorption spectra of the suspensions of other substrate materials are meaningless, because in those substrate materials all the Ag NPs were deposited on the surface of the silica microspheres (LoBs) with an average diameter of 25 μm and the Ag surface plasmon band was screened by the strong scattering from the silica microspheres (Fig. S11). As indicated in the experimental method, the color of aqueous dispersion of LoBs was gray white, whereas the dispersion of LoBs@Ag displayed a black color, being quietly different from the bright yellow color of the Ag colloids. This difference is attributed to the coating of Ag NPs on the surface of LoBs microspheres. We treated the dispersion of LoBs@Ag by adding excessive HF, which dissolved fully the silica microspheres and released the deposited Ag particles. After the HF treatment, it was observed that the color of the dispersion turned to light yellow. This indicated that the Ag particles deposited on the surface of LoBs microspheres were in the form of NPs without observable agglomeration.

The morphology of the obtained Ag NPs on different substrates was checked with the aids of high-resolution SEM images (Fig. S12). On the LoB@Ag surface (Figs. S12-a and b), the Ag NPs were well distributed with a high coverage density, and the Ag NPs were monodisperse with an average diameter of about 12 nm, the "assembling" of which made the Ag NP layer look like a curtain consisting of beads. The use of APTES as a coupling agent decreased the coverage density of Ag NPs, and increased the average diameter of Ag NPs to about 80 nm (Figs. S12-c and d). Similar effect was observed when DA was used as a coupling agent (Figs. S12-e, g, and h), which increased the average diameter of Ag NPs to 70 nm (LoBs@PDA@Ag-R) or 105 nm (LoBs@PDA@Ag-A). As for the Ag colloid prepared with $NH_2OH{\cdot}HCl$ as the reducing agent, the Ag NPs displayed an uniform distribution with an average diameter of 50 nm (Fig. S12-f), being well consistent with the particle size analysis of Ag colloid (Fig. S13). In short, the LoB@Ag substrate, among all the tested substrate materials, provided Ag NPs with the highest coverage density, the best size distribution and smallest average particle size, which may be the most important reason for the strong Raman enhancing effect of the LoB@Ag substrate. To further confirm it, the coverage density of surface Ag NPs was increased by increasing the concentration of Ag^+ used in the preparation of the substrate material. It was clearly seen that when the Ag^+ concentration was increased from 0.001 to 0.01 mol L^{-1}, the SERS intensity of CV at 1619 cm^{-1} is greatly increased (Fig. S14). However, when the Ag^+ concentration was further increased to 0.03 mol L^{-1}, a serious agglomeration of Ag NPs happened (Fig. S15), resulting in rapid decreasing in the SERS intensity. This is also the reason for that the Ag^+ concentration was selected at 0.01 mol L^{-1} in the present work.

Moreover, we noted that a serious problem is that the Raman peaks provided by either LoBs@APTES@Ag or LoBs@PDA@Ag-A are very broad. This indicates that the resolution of these two substrates is very poor even their enhancing effects are promising. The poor resolution of these two substrates is possibly related to the use of the coupling agent, which easily lead to interference in the Raman signals. By comparing the Raman spectra on LoBs, LoBs@Ag, LoBs@PDA and LoBs@PDA@Ag-A (Fig. S16), it was found that the Raman peaks of PDA may be partially overlapping the characteristic Raman peaks of CV in the region of 800 ~ 2000 cm^{-1}. When the Ag NPs were deposited on the surface of LoBs@PDA by the chemical reduction with the use of $NaBH_4$ instead of simply adsorbing of Ag^+, LoBs@PDA@Ag-R was obtained as the substrate. In comparison with LoBs@PDA@Ag-A, indeed, LoBs@PDA@Ag-R improved the resolution of the Raman spectrum of CV, along with further increasing the Raman intensity. The SERS response requires the adsorption of a reporter (CV molecule) on the Ag surface, but the coupling agent can displace parts of the would-be adsorbed CV molecules, causing a loss of the Raman spectroscopic signatures[48]. Therefore, the SERS intensity of CV on these substrates with the use of coupling agents (LoBs@APTES@Ag, LoBs@PDA@Ag) is obviously lower than that on the LoBs@Ag substrate.

On the basis of the above discussions, it is found that there are strong Raman vibrational peaks with well defined and high resolution on LoBs@Ag as the substrate. It is attributed to that the LoBs@Ag substrate not only immobilizes well-distributed Ag NPs on the surface LoBs, but also excludes the interference of coupling agents. These advantages make the LoBs@Ag substrate exhibit a strong Raman enhancing effect.

In summary, LoBs@Ag as a SERS substrate was successfully obtained with a one-pot method without using any coupling agent, and its enhancing SERS effect was investigated by using CV as a probe. By the SERS measurement and DFT calculations, the adsorption of CV on the LoBs@Ag substrate was clarified. On the basis of the surface selection rule, the enhancements of both in-plane and out-of-plane modes suggest that CV adsorbs on LoBs@Ag substrate surface through its N atom with one phenyl ring of CV tilted with respect to the LoBs@Ag surface. Comparing with other substrates, all Raman peaks of CV on the LoBs@Ag substrate were obviously enhanced without any interference peak. In comparison with normal Raman scattering, the LoBs@Ag substrate provided an enhancing factor as high as 6.9×10^8 for CV, which is much more than that provide by Ag colloid ($\sim 3.1 \times 10^6$) and the Ag-coated LoBs with the use of coupling agents (about 2×10^7). The LoBs@Ag substrate exhibited excellent reproducibility and stability, broad adaptability. With LoBs@Ag as the substrate, the linear-response range for CV was wider than that in previous reports. The LoBs@Ag-based SERS method will have promising applications in rapid analysis of organic pollutants and small bio-molecules.

Methods

Reagents and materials. CV, DA, silver nitrate ($AgNO_3$), solium borohydride ($NaBH_4$), sodium hydroxide (NaOH), ammonium persulfate ($NH_4S_2O_8$, AP), hydroxylamine hydrochloride ($NH_2OH{\cdot}HCl$), hydrochloric acid (HCl) were purchased from Sinopharm Chemical Reagent Co. Ltd. APTES, guanine and trihydroxymethyl aminomethane (Tris) were obtained from Aladdin Chemical Co. Ltd. Paraquat was purchased from Hubei Sanonda Co. Ltd. Tianmen Agrochemical Plant. All the chemicals were of analytical grade and were used as received. LoBs were supplied by 3 M Corporation. Milli-Q water (18.2 MΩ·cm) provided by a Milli-Q Labo apparatus (Thermo Fischer Scientific) was used in all experiments.

Characterization. The morphology, size and surface chemical compositions of LoBs were examined with a scanning electron microscope (SEM, JSM-5510LVA, Japan), a field emission scanning electron microscope (FEI Nova NanoSEM), a transmission electron microscope (TEM, FEI Tecnai G20, USA) and an energy-dispersive spectroscopy (EDS, EDAX-FALCON60, USA), respectively. The size distribution of LoBs was characterized with a laser particle size analyzer (LPSA, Winner-2000ZD, China). Zeta potentials and particle size analysis were measured on a Nano-ZS90 zetasizer instrument (Malvern). The crystallinity was determined on a X-rays diffractometer (XRD; Bruker D8 Advance TXS) equipped with Cu Kα radiation (λ = 1.54 Å) source (applied voltage 40 kV, current 40 mA). Scans were recorded for 2θ values between 10° and 70°, using a step size of 0.02° and integration of 16 s per step. UV-visible absorption spectra were recorded on a Shimadzu UV-2550 spectrophotometer (Kyoto, Japan). FTIR spectra were acquired on a Nicolet 6700 FT-IR spectrometer (American Thermo Electron). Raman spectra were measured on a confocal laser micro-Raman spectrometer (Thermo Fischer DXR, USA) equipped with a He-Ne laser of excitation of 532 nm (laser serial number: AJC1200566). The laser was focused onto the substrate with an Olympus ×50 long distance objective. The radius of illumination laser spot size was ~0.55 μm. Samples were mounted on an automatic stage allowing the control of 1 μm step size. Spectra were obtained at a laser power of 3 mW and a 2 s acquisition time with 900 lines/mm grating (Grating serial number: AJG1200531) in the wavenumber range of 50 ~ 3500 cm^{-1}. Baseline corrections were carried out to correct the optical background signal from the substrate.

Preparation of SERS substrates. Ag colloid: A total of 40 mL of NaOH solution (7.5 mmol L^{-1}) was added to 50 mL of a hydroxylamine hydrochloride solution (3.0 mmol L^{-1}). Then 10 mL of $AgNO_3$ aqueous solution (10 mmol L^{-1}) was rapidly added to the mixture under ultrasound irradiation with a powder of 140 W. After 5 min, a milky gray color colloid was obtained and stored in a refrigerator at 4°C for further use.

LoBs@Ag: It was prepared by directly reducing $AgNO_3$ in LoBs suspension at room temperature. 0.4 g of S60-HS LoBs (density 0.6 g mL^{-1}) was first washed and flotated in 200 mL H_2O. The LoBs flotation was added in 30 mL H_2O under vigorous stirring. Then 10 mL of 0.01 mol L^{-1} $AgNO_3$ solution and 10 mL of 0.026 mol L^{-1} $NaBH_4$ solution were successively added into the above suspension. The white suspension changed to dark immediately after adding the $NaBH_4$ solution. A few minutes later, the mixture changed to brownish yellow and finally to black. After stirring for 1 h, the LoB@Ag were obtained by filtering through a vacuum filter fitted with a 0.22 μm microporous membrane. Then the LoBs@Ag was thoroughly rinsed with Milli-Q water and dispersed in 30 mL Milli-Q water before morphological/structural characterizations and SERS evaluations.

LoBs@APTES@Ag: LoBs@APTES@Ag was prepared by the method reported by Schmit et al[19]. LoBs were first activated by APTES. Colloidal Ag was then incubated with the LoBs, resulting in Ag NPs aggregation onto the activated LoBs surface.

LoBs@PDA@Ag: LoBs@PDA@Ag-R was prepared by the method reported by Wei et al[49], in which Ag NPs were directly reduced by PDA. A given amount of the flotated LoBs was added in 50 mmol L^{-1} Tris-HCl buffer solution (pH = 8.5) under magnetic stirring. DA and AP (the molar ratio of AP to DA was 1 : 2) were successively added into the mixture. Due to the polymerization of DA, the colour of the mixture changed to brown after stirring for 20 min. The resultant mixture was filtered and washed. Then the coated LoBs (LoBs@PDA) were added in 50 mL H_2O under vigorous stirring. This mixture was defined as mixture-1. 0.1 mmol $AgNO_3$ and a small amount of $NaBH_4$ were successively added into mixture-1. After stirring for 2 h, the LoBs@PDA@Ag-R was prepared. Meanwhile, the synthesized Ag colloid was added into the mixture-1. After stirring for 12 h, the LoBs@PDA@Ag-A (Ag NPs were absorbed by PDA.) was obtained. The LoBs@PDA@Ag was filtered, rinsed and dispersed in 30 mL Milli-Q water for use.

Computational details. Theoretical calculations concerning the geometry optimization and the Raman spectra were performed by using Gaussian09 software package[50], implemented on an Intel Pentium PC computer with 3.50 GHz processor and 16 GB of memory. Optimization of the molecular structures and vibration Raman spectra calculations for the optimized structures were performed by means of density functional theory (DFT) with the Becke's 3 parameters and the Lee-Yang-Parr's nonlocal correlation functional (B3LYP). The basis sets for C, N and H were 6-311 + G (d) with diffuse function only for N atoms. For silver atoms, the valence and core electrons were described by the pseudopotential LanL2DZ basis set. The solvent (water) effect was considered by the conductor-like polarized continuum model (CPCM). For comparison of theoretical and experimental data, all the calculated Raman frequencies were scaled by a factor 0.96 due to the correction of the harmonic approximation and the incomplete DFT approaches. The intensities of the Raman bands were estimated by calculating the differential Raman scattering cross-section.

1. de Melo, V. H. S., Zamarion, V. M., Araki, K. & Toma, H. E. New insights on surface-enhanced Raman scattering based on controlled aggregation and spectroscopic studies, DFT calculations and symmetry analysis for 3,6-bi-2-pyridyl-1,2,4,5-tetrazine adsorbed onto citrate-stabilized gold nanoparticles. *J. Raman Spectrosc.* **42**, 644–652 (2011).
2. Yang, K. H., Liu, Y. C. & Yu, C. C. Enhancements in intensity and stability of surface-enhanced Raman scattering on optimally electrochemically roughened silver substrates. *J. Mater. Chem.* **18**, 4849–4855 (2008).
3. Liu, Y. C. Evidence of chemical effect on surface-enhanced Raman scattering of polypyrrole films electrodeposited on roughened gold substrates. *Langmuir* **18**, 174–181 (2002).
4. Ayas, S. *et al.* A. Label-free nanometer-resolution imaging of biological architectures through surface enhanced Raman scattering. *Sci. Rep.* **3**, 2624; DOI:10.1038/srep02624 (2013).
5. Liu, H. *et al.* Single molecule detection from a large-scale SERS-active $Au_{79}Ag_{21}$ substrate. *Sci. Rep.* **1**, 112; DOI:10.1038/srep00112 (2011).
6. Fleischmann, M., Hendra, P. J. & McQuillan, A. J. Raman-spectra of pyridine adsorbed at a silver electrode. *Chem. Phys. Lett.* **26**, 163–166 (1974).
7. Pettinger, B., Wenning, U. & Wetzel, H. Surface plasmon enhanced Raman scattering frequency and angular resonance of Raman scattered light from pyridine on Au, Ag and Cu electrodes. *Surf. Sci.* **101**, 409–416 (1980).
8. Moskovits, M. Surface roughness and the enhanced intensity of Raman scattering by molecules adsorbed on metals. *J. Chem. Phys.* **69**, 4159–4161 (1978).
9. Hexter, R. M. & Albrecht, M. G. Metal surface Raman spectroscopy: theory. *Spectrochim. Acta. A.* **35**, 233–251 (1979).
10. Moskovits, M. Surface-enhanced Raman spectroscopy: a brief retrospective. *J. Raman Spectrosc.* **36**, 485–496 (2005).
11. Jeon, H. C., Heo, C. J., Lee, S. Y., Park, S. G. & Yang, S. M. Optically tunable arrayed structures for highly sensitive plasmonic detection via simplified holographic lithography. *J. Mater. Chem.* **22**, 4603–4606 (2012).
12. Lee, S. Y., Jeon, H. C. & Yang, S. M. Unconventional methods for fabricating nanostructures toward high-fidelity sensors. *J. Mater. Chem.* **22**, 5900–5913 (2012).
13. Heo, C. J. *et al.* Robust plasmonic sensors based on hybrid nanostructures with facile tunability. *J. Mater. Chem.* **22**, 13903–13907 (2012).
14. Yang, M. *et al.* SERS-active gold lace nanoshells with built-in hotspots. *Nano Lett.* **10**, 4013–4019 (2010).
15. Liu, B. *et al.* Shell thickness-dependent Raman enhancement for rapid identification and detection of pesticide residues at fruit peels. *Anal. Chem.* **84**, 255–261 (2012).
16. Peng, P., Huang, H., Hu, A., Gerlich, A. P. & Zhou, Y. N. Functionalization of silver nanowire surfaces with copper oxide for surface-enhanced Raman spectroscopic bio-sensing. *J. Mater. Chem.* **22**, 15495–15499 (2012).
17. van Lierop, D., Larmour, I. A., Faulds, K. & Graham, D. SERS primers and their mode of action for pathogen DNA detection. *Anal. Chem.* **85**, 1408–1414 (2013).
18. Schmit, V. L., Martoglio, R., Scott, B., Strickland, A. D. & Carron, K. T. Lab-on-a-bubble: synthesis, characterization, and evaluation of buoyant gold nanoparticle-coated silica spheres. *J. Am. Chem. Soc.* **134**, 59–62 (2012).
19. Schmit, V. L., Martoglio, R. & Carron, K. T. Lab-on-a-bubble surface enhanced Raman indirect immunoassay for cholera. *Anal. Chem.* **84**, 4233–4236 (2012).
20. Park, J. H. *et al.* Fabrication of hollow silver spheres by MPTMS-functionalized hollow silica spheres as templates. *Mater. Res. Bull.* **40**, 271–280 (2005).
21. Lee, H., Dellatore, S. M., Miller, W. M. & Messersmith, P. B. Mussel-inspired surface chemistry for multifunctional coatings. *Science* **318**, 426–430 (2007).
22. Wang, L. Y. *et al.* Silver nanoparticles assembled on mica and its surface-enhanced Raman scattering effect. *Chem. J. Chinese Universities*, **23**, 2169–2171 (2002).
23. Ito, M. & West, R. New aromatic anions. IV. vibrational spectra and force constants for $C_4O_4^{-2}$ and $C_5O_5^{-2}$. *J. Am. Chem. Soc.* **85**, 2580–2584 (1963).
24. Lai, K. Q. *et al.* Determination of chloramphenicol and crystal violet with surface enhanced Raman spectroscopy. *Sens. Instrumen. Food Qual.* **5**, 19–24 (2011).
25. Meng, W. *et al.* SERS and DFT study of crystal violet. *J. Mol. Struct.* **1035**, 326–331 (2013).
26. Kleinman, S. L. *et al.* Single-molecule surface-enhanced Raman spectroscopy of crystal violet isotopologues: theory and experiment. *J. Am. Chem. Soc.* **133**, 4115–4122 (2011).
27. Wang, D., Zhu, W., Best, M. D., Camden, J. P. & Crozier, K. B. Wafer-scale metasurface for total power absorption, local field enhancement and single molecule Raman spectroscopy. *Sci. Rep.* **3**, 2867; DOI:10.1038/srep02867 (2013).
28. Le Ru, E. C., Blackie, E., Meyer, M. & Etchegoin, P. G. Surface enhanced Raman scattering enhancement factors: a comprehensive study. *J. Phys. Chem. C.* **111**, 13794–13803 (2007).
29. Chakraborty, I., Bag, S., Landman, U. & Pradeep, T. Atomically precise silver clusters as new SERS substrates. *J. Phys. Chem. Lett.* **4**, 2769–2773 (2013).
30. Kudelski, A. Raman studies of Rhodamine 6G and crystal violet sub-monolayers on electrochemically roughened silver substrates: do dye molecules adsorb preferentially on highly SERS-active sites? *Chem. Phys. Lett.* **414**, 271–275 (2005).
31. Gao, P. & Weaver, M. J. Surface-enhanced Raman spectroscopy as a probe of adsorbate-surface bonding: benzene and monosubstituted benzenes adsorbed at gold electrodes. *J. Phys. Chem.* **89**, 5040–5046 (1985).
32. Hu, G. S. *et al.* Charge transfer between triphenyl phosphine and colloidal silver: a SERS study combined with DFT calculations. *J. Phys. Chem. C.* **111**, 8632–8637 (2007).
33. Moskovits, M. & Suh, J. S. Conformation of mono-and dicarboxylic acids adsorbed on silver surfaces. *J. Am. Chem. Soc.* **107**, 6826–6829 (1985).
34. Moskovits, M. Surface-enhanced spectroscopy. *Rev. Mod. Phys.* **57**, 783–826 (1985).
35. Alonso-González, P. *et al.* Resolving the electromagnetic mechanism of surface-enhanced light scattering at single hot spots. *Nat Commun.* **3**, 684 (2012).

36. Hu, G. S. *et al.* Adsorption of ethanediamine on colloidal silver: a surface-enhanced Raman spectroscopy study combined with density functional theory calculations. *J. Phys. Chem. C.* **111**, 11267–11274 (2007).
37. Fernández-López, C. *et al.* Highly controlled silica coating of PEG-capped metal nanoparticles and preparation of SERS-encoded particles. *Langmuir* **25**, 13894–13899 (2009).
38. Li, J. M. *et al.* Poly(styrene-co-acrylic acid) core and silver nanoparticle/silica shell composite microspheres as high performance surface-enhanced Raman spectroscopy (SERS) substrate and molecular barcode label. *J. Mater. Chem.* **21**, 5992–5998 (2011).
39. Jeon, H. J., Yi, S. C. & Oh, S. G. Preparation and antibacterial effects of Ag-SiO_2 thin films by sol-gel method. *Biomaterials* **24**, 4921–4928 (2003).
40. Kang, S. *et al.* Preparation and characterization of epoxy composites filled with functionalized nanosilica particles obtained via sol–gel process. *Polymer* **42**, 879–887 (2001).
41. Yang, H. M., Li, M., Fu, L. J., Tang, A. D. & Mann, S. Controlled assembly of Sb_2S_3 nanoparticles on silica/polymer nanotubes: insights into the nature of hybrid interfaces. *Sci. Rep.* **3**, 1336; DOI:10.1038/srep01336 (2013).
42. Zhang, Y., He, X., Ouyang, J. & Yang, H. M. Palladium nanoparticles deposited on silanized halloysite nanotubes: synthesis, characterization and enhanced catalytic property. *Sci. Rep.* **3**, 2948; DOI:10.1038/srep02948 (2013).
43. Kathi, J. & Rhee, K. Y. Surface modification of multi-walled carbon nanotubes using 3-aminopropyltriethoxysilane. *J Mater Sci* **43**, 33–37 (2008).
44. Hoang, C. V., Oyama, M., Saito, O., Aono, M. & Nagao, T. Monitoring the presence of ionic mercury in environmental water by plasmon-enhanced infrared spectroscopy. *Sci. Rep.* **3**, 1175; DOI:10.1038/srep01175 (2013).
45. Sun, X. P. & Wei, W. T. Electrostatic-assembly-driven formation of micrometer-scale supramolecular sheets of (3-aminopropyl) triethoxysilane (APTES)-HAuCl4 and their subsequent transformation into stable APTES bilayer-capped gold nanoparticles through a thermal process. *Langmuir* **26**, 6133–6135 (2010).
46. Kobayashi, Y., Salgueiri¯n O-Maceira, V. & Liz-Marzán, L. M. Deposition of silver nanoparticles on silica spheres by pretreatment steps in electroless plating. *Chem. Mater.* **13**, 1630–1633 (2001).
47. Zhang, L. F. *et al.* Electrospun nanofibrous membranes surface-decorated with silver nanoparticles as flexible and active/sensitive substrates for surface enhanced Raman scattering. *Langmuir* **28**, 14433–14440 (2012).
48. Doering, W. E. & Nie, S. Spectroscopic tags using dye-embedded nanoparticles and surface-enhanced Raman scattering. *Anal. Chem.* **75**, 6171–6176 (2003).
49. Wei, Q., Zhang, F., Li, J., Li, B. & Zhao, C. Oxidant-induced dopamine polymerization for multifunctional coatings. *Polym. Chem.* **1**, 1430–1433 (2010).
50. Frisch, M. J. *et al.* Gaussian 09. Revision A.1. Gaussian, Inc., Wallingford, CT (2009).

Acknowledgments

This work was financially supported by the National High Technology Research and Development Program of China (863 Program) (Grant No. 2012AA06A304), the National Science Foundation of China (Grant Nos. 21177044 and 21377169), and the Scientific Research Key Project of Hubei Provincial Department of Education (Project No. D20121503). The Analytical and Testing Center of Wuhan Institute of Technology is thanked for its help in the characterization of the substrates.

Author contributions

J.Z.J., L.H.Z. and H.Q.T. designed experiments and wrote the manuscript; J.Z.J. carried out most experiments. L.O.-Y. and J.Z. carried parts of the experiments. All authors discussed the results.

Additional information

Supplementary information accompanies this paper at http://www.nature.com/scientificreports

Competing financial interests: The authors declare no competing financial interests.

How to cite this article: Jiang, J.Z., Ou-Yang, L., Zhu, L.H., Zou, J. & Tang, H.Q. Novel One-pot Fabrication of Lab-on-a-Bubble@Ag Substrate without Coupling-agent for Surface Enhanced Raman Scattering. *Sci. Rep.* **4**, 3942; DOI:10.1038/srep03942 (2014).